Polymer Bulletin 51, 85–92 (2003)
DOI 10.1007/s00289-003-0197-1

Polymer Bulletin
© Springer-Verlag 2003

Structure development and isothermal crystallization behaviour of compatibilized PET/expandable fluorine mica hybrid nanocomposite

C.Saujanya, Y.Imai (✉), H.Tateyama

Institute for Structural and Engineering Materials, National Institute of Advanced Industrial Science & Technology (AIST), 807-1, Shuku-machi, Tosu, Saga 841-0052, Japan,
E-mail: y-imai@aist.go.jp, Fax: +81-942-81-3693

Received: 18 June 2003/Accepted: 16 August 2003

Summary

The compatibilized PET/expandable fluorine mica (ME) hybrid nanocomposite (CN) prepared by in situ polymerization technique showed a partially exfoliated structure of ME in PET matrix by XRD analysis, owing to its broad crystalline peak accompanied by an increase of *d*-spacing as compared to PET/ME uncompatibilized composite (UC). The analysis by TEM revealed a better dispersion of ME in PET for CN as compared to aggregates of ME in case of UC. Further, the isothermal crystallization behaviour studied using DSC for the same at different crystallization temperature (T_c) revealed a significant decrease of crystallization half time and remarkable increase of crystallization rates (almost 2 times than pure PET) for CN in contrast to UC. The Avrami exponent n lowered to 2.3 for CN as compared to 3.1–3.4 for pure PET at various T_c. The activation energy (E_a) determined from Arrhenius equation reduced dramatically for CN. These various observations could be explained based on the nucleation efficiency by ME accompanied by different crystallization/growth process occurring in case of hybrid nanocomposite.

Introduction

A number of papers are being cited these days in the literature in the field of hybridization of polymer/clay nanocomposites owing to their unique properties such as high modulus and strength, improved barrier properties, increase in solvent and heat resistance, reduced flammability, good optical transparency etc even at very low quantities of clay compared to conventional polymer microcomposites [1–4]. Recently, a new approach, the use of a compatibilizer, to prepare exfoliated polymer/clay hybrid nanocomposite has gained considerable attention amongst the various groups [5–7]. Thus, in all their works; the authors have mainly focused on the synthetic methodologies and addressed primarily the morphology, rheology and remarkable enhancements in mechanical, thermal and other properties.
In this scenario, a few attempts have been made to study the isothermal crystallization behaviour of dispersed clay nanocomposites which are very important from the processing point of view especially in optimizing the processing conditions, in

correlating the structure–property relationships and also critical in achieving accurate value of Avrami exponent 'n' which provides information on the type of nucleation and crystal growth geometry. A few authors have studied the function of inorganic nanofillers such as silica, montmorillonite (MMt), or calcium phosphate on the isothermal crystallization behaviour of base polymers such as polystyrene [8], polypropylene [9], polyamide 6 [10] etc and have shown that the addition of small amount of nanofiller in polymer plays a strong nucleating role affecting greatly the crystallization rate and crystallization half time of polymer. However, very few experiments [11,12] to study the effect of nanofiller on the isothermal crystallization of PET, an industrially important polymer, have been noted where the authors have mainly used organically modified natural montmorillonite (MMt) clay and have shown significant improvement as a nucleating agent. In our present investigation, we have used expandable synthetic mica clay [13] dispersed in PET. This clay is more superior than natural MMt clay in two ways: (1) the synthetic mica clay has a higher net negative charge of about 0.7 per formula unit on its surface compared to natural MMt clay which is about 0.3 and (2) this higher net negative charge in the former case can promote relatively more adsorption of long chain cationic surfactant leading to greater expansion of interlayer distance. Therefore, the polymer can be expected to be intercalated/delaminated to an enormous extent compared to the latter. Thus, the interfacial compatibility between PET–ME could be expected to be better compared to PET–MMt clay which in turn can greatly affect the crystallization of PET.
With this asset, in the present article, we report the role of ME on the isothermal crystallization of PET prepared by in situ polymerization method in presence of a compatibilizer. In the first part, the nanocomposite structure is investigated by XRD and TEM techniques. In the second part, the isothermal crystallization of PET using DSC is discussed followed by the determination of activation energy parameter (E_a) by Arrhenius equation. The results obtained for CN is compared with UC and pure PET.

Experimental:

The nanocomposite of PET/ME hybrid by in situ polymerization method with a novel compatibilizer 10-[3,5-bis(methoxycarbonyl)phenoxy]decyltriphenylphosphonium bromide (IP10TP) was successfully prepared (in the same way as described in our previous paper [5]) by intercalation of low content of IP10TP (0.2 mmole/g-ME) into ME by cation exchange reaction followed by melt polymerization of bis(2-hydroxyethyl)terephthalate (BHET) in the presence of IP10TP/ME intercalation compound. The content of ME with respect to BHET was kept at 4wt%. Subsequently solid state polymerization [14] was employed to increase the molecular weight. The same procedure was utilized for preparing PET/ME without IP10TP (UC) and pure PET for comparison. The molecular weights of these samples were maintained nearly same (M_n of pure PET = 9,400, UC = 10,300 and CN = 8,400) prior to the crystallization study.
The characterization of nanocomposite structure of ME in PET was investigated by XRD and TEM techniques. The XRD patterns were recorded with an X-ray diffractometer (Philips, X'Pert) equipped with Cu Kα radiation (0.1541 nm). The TEM micrographs were taken from a microtomed section of 50 nm thick samples mounted in epoxy with a transmission electron microscope (JEM-200CX, JEOL Co.,

Japan) with an acceleration voltage of 120 kV.
The isothermal crystallization behaviour was analysed on a Seiko instrument (SII DSC-6200 model), which was calibrated using indium as the reference. The experiments were carried out under nitrogen. The samples (about 10 mg) were heated to 300 °C at a rate of 20 °C/min and held for 5 min to remove the residual crystals, then they were rapidly quenched at a maximum cooling rate (60 °C/min) to reach the proposed T_c (208, 213, 218, 223 °C) and the crystallization exotherm was monitored as a function of time until the crystallization was completed. The results obtained for CN were compared with that of UC and pure PET. In addition, the activation energy parameter (E_a) was determined for these samples by Arrhenius equation.

Results and discussion

Figure 1 presents the WAXD scans for compatibilized hybrid nanocomposite (CN) containing low content of IP10TP (0.2 mmole/g ME) represented by the curve C while curve B corresponds to PET/ME without IP10TP (UC) and curve A that of pure PET. It is apparent that the CN shows an increase in the interlamellar distance of $d_{001}$of ME of 1.96 nm (marked as arrow 1) compared with the interlamellar distance of original ME of 0.96 nm while for UC the interlamellar distance increased to only 1.25 nm. Further, the extent of broadening in case of CN clearly shows significantly small size of ME crystallites compared to UC. In addition, broadening is observed even for PET peak (marked as arrow 2) of CN as compared to pure PET. The crystallite size was determined by Scherrer's formula, which was reported in our previous paper [15]. The crystallite size of ME reduced to 8 nm for CN compared to 45 nm for UC and also the crystallite size of PET dropped down to 3.7 nm compared to 9.7 nm for Pure PET. These observations suggests that the ME layers in the presence of a compatibilizer could be partially exfoliated into the PET/clay hybrid.

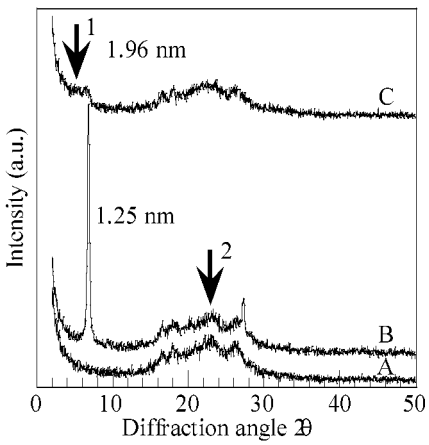

Figure 1. WAXD scans for compatibilized PET/ME hybrid nanocomposite represented by the curve C, PET/ME without IP10TP by curve B and Pure PET by curve A.

In order to confirm the degree of dispersion of ME in PET for CN, the TEM analysis was performed, the micrographs of which are depicted below (Fig.2). The UC micrograph (a) shows poor dispersion of ME in PET due to the distinct formation of

aggregates of ME stacked together in clusters of average particle size i.e. the thickness is greater than 350 nm and lengthwise it is in the range of 2.5–3 μm giving rise to a microcomposite. While the morphology of CN micrograph (b) shows a better dispersion of ME crystallites in PET with few agglomerates and the particle size i.e. thickness drops down to 50–100 nm on an average and along lengthwise to 0.25–0.5 μm compared to UC. Thus, it is clear that the dispersibility of ME in case of CN is much improved in the presence of a compatibilizer leading to nanoscale dispersion of ME in PET matrix.

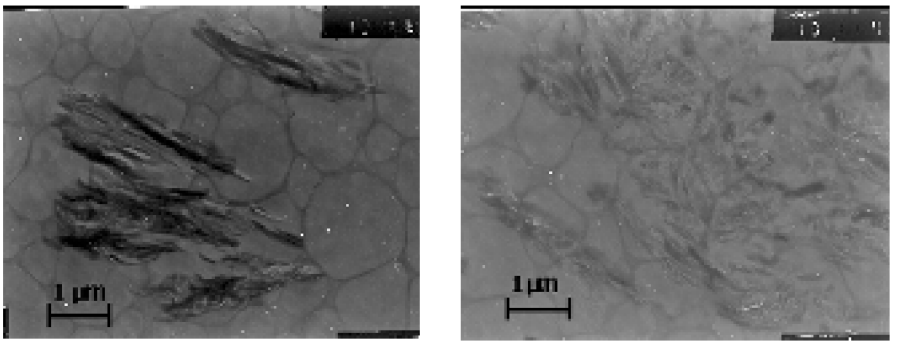

(a) (b)

Figure 2. The TEM micrographs for (a) UC and (b) CN

The isothermal crystallization behaviour for these samples were studied using DSC at different T_c (208–223 °C). Figure 3 shows the plots of relative crystallinity, X_t elucidated from the DSC thermograms as a function of time t for I) pure PET, II) UC and III) CN at different T_c. The degree of crystallinity (excluding the induction time) was determined by using Avrami equation [16] as

$$X_t = \int_0^t (dH_c/dt)dt \Big/ \int_0^\infty (dH_c/dt)dt = 1 - \exp(-kt^n) \qquad (1)$$

Where X_t is the weight fraction of a material crystallized at time t, dH_c/dt is the rate of crystallization heat evolution. The parameter k in eqn (1) is an overall crystallization rate constant and n is the Avrami exponent that provides information on the type of nucleation and crystal growth geometry. It is obvious from the figure (a–d) that the crystallization proceeds rapidly for CN (III) with the slope of the curve becoming more steep compared to UC (II). While for pure PET, the crystallization proceeds rather slowly with increase in T_c. The crystallization half time ($t_{1/2}$) and the crystallization rates $\tau_{1/2}$ (reciprocal of $t_{1/2}$) were determined from these curves listed in Table 1. Higher crystallization rates with a drastic reduction in $t_{1/2}$ value are observed for CN at different T_c and the rates of crystallization for CN are accelerated by 1.5 times than UC and almost 2 times than pure PET at different T_c. In case of PET with 5 wt% modified MMt clay [12] the crystallization rate improved by only 1.3 times than

pure PET at 210 °C. While Y.C.Ke et al [11] showed that the crystallization patterns of PET affected up to an MMt content of 3 wt%. In our experimental observations, it is obvious that ME exhibits an effective nucleating agent for PET. Further, the higher crystallization rates observed in case of CN (at 4 wt% ME) can be associated with substantial enhancement of nucleation efficiency developed which can be further attributed due to two factors: Firstly, the nanoscale dispersion of ME layers in PET matrix facilitated at the low content of compatibilizer (IP10TP), which provides better interfacial interaction between PET and ME. Secondly, the nanocrystallites of ME which offers greater nucleation efficiency due to high active surface area on the crystallization of PET, compared to nucleation ability enabled by the microcrystallites of ME in case of UC.

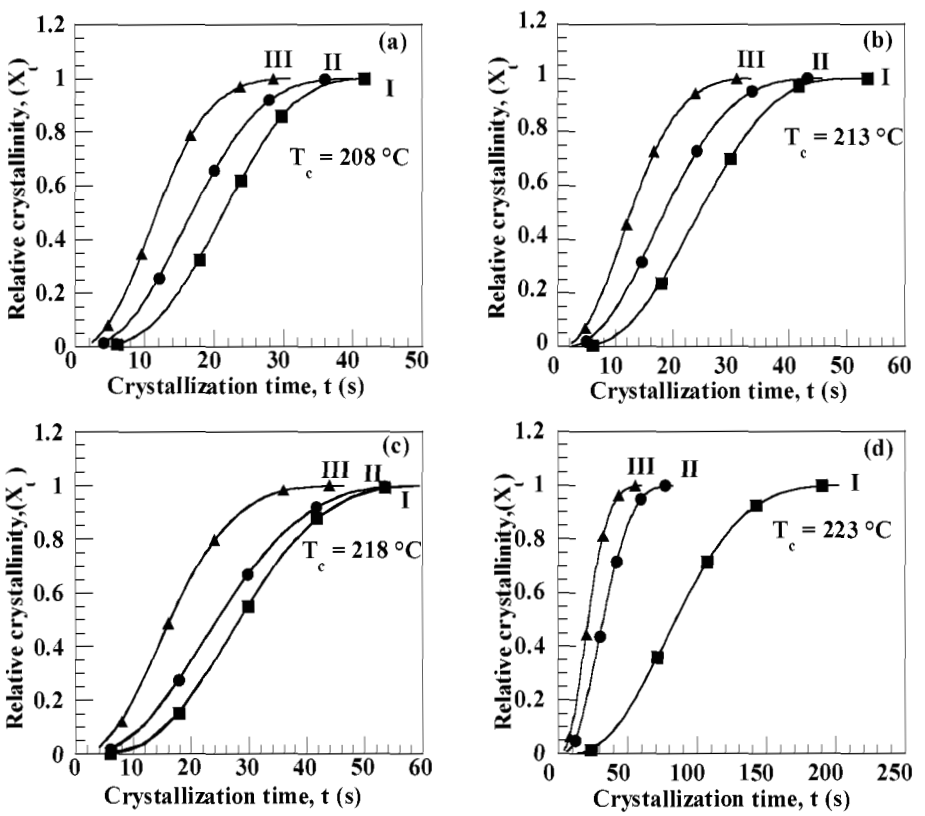

Figure 3. Plots of relative crystallinity with time for isothermal crystallization of I) Pure PET, II) UC and III) CN at different T_c as denoted by the symbols (a–d).

Table 1. Isothermal Crystallization data for compatibilized PET/ME hybrid nanocomposite

Sample	T_c (°C)	$t_{1/2}$ (s)	$\tau_{1/2}$ (s^{-1})	k (s^{-1})	n	ΔH_c (J/g)	E_a (kJ/mol)
Pure PET	208	21.7	0.046	3.16×10^{-5}	3.3	-2.25	-162.1
	213	24.7	0.040	1.50×10^{-5}	3.3	-3.37	
	218	28.6	0.035	5.60×10^{-6}	3.4	-2.69	
	223	86.5	0.012	4.07×10^{-7}	3.1	-13.01	
UC	208	17.1	0.058	4.27×10^{-4}	2.6	-26.45	-78.9
	213	18.5	0.054	3.56×10^{-4}	2.6	-26.54	
	218	24.7	0.040	1.90×10^{-4}	2.6	-25.16	
	223	33.0	0.030	8.31×10^{-5}	2.6	-24.07	
CN	208	11.9	0.084	2.37×10^{-3}	2.3	-29.89	-66.4
	213	12.7	0.079	1.98×10^{-3}	2.3	-30.26	
	218	16.5	0.060	1.08×10^{-3}	2.3	-26.90	
	223	22.0	0.045	5.80×10^{-4}	2.3	-25.16	

Figure 4 represents the Avrami plots for I) pure PET, II) UC and III) CN at different T_c. All the curves are fitted well by the Avrami equation (1) and result in linear relationships. The Avrami exponent n and overall crystallization rate constant k were determined from the slopes and intercepts of the linear plots, which are shown in Table 1. For pure PET, the Avrami exponent n of 3.1–3.4 at different T_c clearly shows three dimensional formation of spherulitic growth. However, for UC and CN, the value of n decreases to 2.6 and 2.3, respectively, at different T_c. The lower value of n strongly signifies the two dimensional crystallization of PET due to heterogeneous nucleation by ME platelets. The further decrease of n value of 2.3 for CN at various T_c could be ascribed due to high nucleation density furnished by the nanosize ME crystallites as explained earlier. In addition, the overall crystallization rate constant k is also found to be exceptionally higher for CN than UC and pure PET.

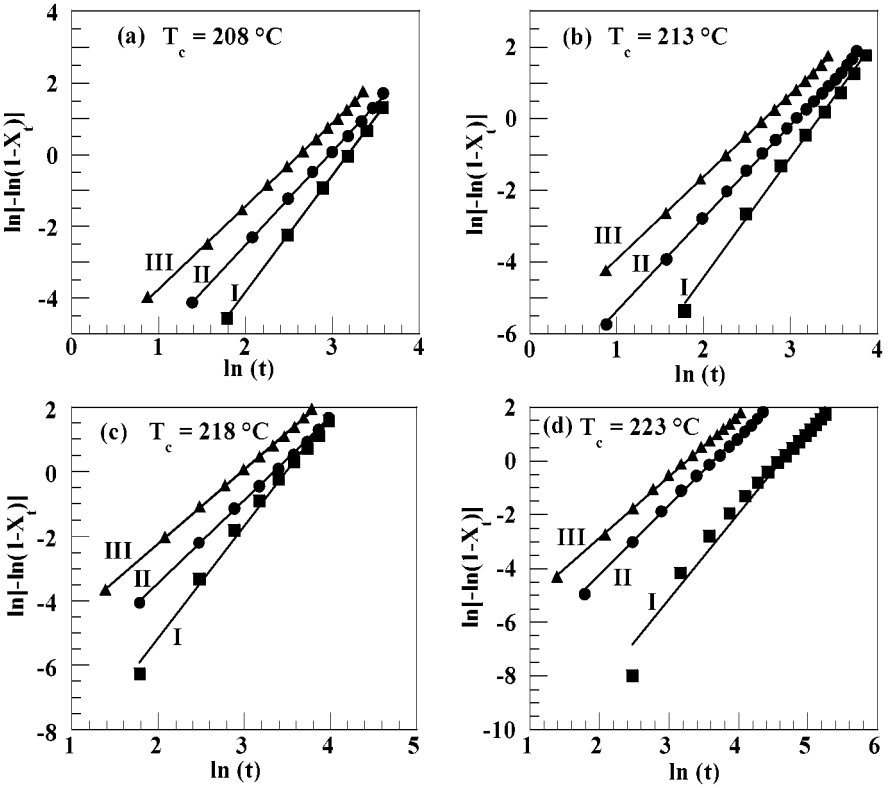

Figure 4. Plots of ln [-ln (1-X_t)] versus ln (t) in (s) for isothermal crystallization of I) Pure PET, II) UC and III) CN at various T_c as denoted by the symbols (a–d).

Table 1 shows the heat of crystallization (ΔH_c) determined from the area of the crystallization peak under the DSC curve. The ΔH_c value for CN is found to increase at different T_c as compared to UC and pure PET thus suggesting higher crystallinity in the former case.

The most distinct feature of the present investigation is the activation energy (E_a) (see Table 1) determined from the slope of the plots of $1/n$ ln k VS $1/T$ by Arrhenius equation [17] as

$$1/n \ln k = \ln k_0 - \Delta E_a / RT \qquad (2)$$

where k is a crystallization rate, k_0 is a temperature independent preexponential factor; ΔE_a is a total activation energy barrier for the transition from melt state to crystalline state, R is the universal gas constant and T is the absolute temperature. The E_a data in Table 1 for pure PET shows a value of 162.1 kJ/mole that is reasonably close to previously reported data between 159 to 247 kJ/mole by the other authors [18]. A dramatic reduction in activation energy barrier towards nucleation is observed in the presence of ME clay. It decreases considerably for CN with a value of 66.4 kJ/mole

compared to 78.9 kJ/mole for UC. The remarkable decrease of E_a in case of CN confirms the strong catalytic role played by the nanosize ME crystallites leading to enormous increase of crystallization rate constant.

Conclusions

From these studies it can be illustrated that the PET/ME prepared in the presence of a compatibilizer (CN) by in situ polymerization method renders hybrid nanocomposite structure with nanoscale dispersion of ME in PET as evidenced by XRD and TEM analysis. The isothermal crystallization behaviour studied at 4wt% ME clearly shows decrease of half time and tremendous increase of crystallization rates for CN at different T_c compared to UC resulting in greater nucleation efficiency on the crystallization of PET by the nanosize ME layers. The Avrami exponent n of 2.3 (in case of CN) distinctly shows two dimensional crystallization of PET due to heterogeneous nucleation by the nanosize ME. Further, the improvement of ΔH_c and the dramatic decrease of E_a for CN confirm the strong catalytic role played by the nanosize ME crystallites.

Acknowledgements

This research was financially supported by the Japan Society for the Promotion of Science (Award no. PB01087).

References

1. Giannelis EP (1996) Adv Mater 8:29
2. Alexandre M, Dubois P (2000) Mater Sci Eng 28:1
3. Usuki A, Hasegawa N, Kadoura H , Okamoto T (2001) Nano Lett 1(5):271
4. Pinnavaia TJ, Beall GW (2001) Polymer-Clay Nanocomposites John Wiley & Sons Ltd
5. Imai Y, Nishimura S, Abe E, Tateyama H, Abiko A, Yamaguchi A, Aoyama T, Taguchi H (2002) Chem Mater 14: 477
6. Kawasumi M, Hasegawa N, Kato M, Usuki A, Okada A (1997) Macromolecules 30:6333
7. Zhang G, Shichi T, Takagi K (2003) Materials Letters 57:1858
8. Tseng CR, Lee HY, Chang FC (2001) J Polym Sci, Part B, Polym Phys 39:2097
9. Saujanya C, Radhakrishnan S (2001) Polymer 42:6723
10. Yang F, Ou Y, Yu Z (1998) J Appl Polym Sci 69:355
11. Ke YC, Yang ZB, Zhu CF (2002) J Appl Polym Sci 85:2677
12. Carter CM (2001) SPE-ANTEC Proc 3:3210
13. Tateyama H, Nishimura S, Tsunematsu K, Jinnai K, Adachi Y, Kimura M (1992) Clays Clay Miner 40:180
14. Imai Y, Inukai Y, Tateyama H (2003) Polym J 35:230
15. Saujanya C, Imai Y, Tateyama H (2002) Polymer Bulletin 49:69
16. Schultz JM (1974) Polymer Materials Sci , Prentice Hall, Englewood Cliffs, NJ
17. Cebe P, Hong SD (1986) Polymer 27: 1183
18. Tan S, Su A, Li W, Zhou E (2000) J Polym Sci, Part B, Polym Phys 38:53